Impact of network topology on the thermal and mechanical properties of lithium germanate glasses

Sørensen, Søren S.; To, Theany; Christensen, Johan F.S.; Johra, Hicham; Smedskjaer, Morten M.

Published in:
Journal of the American Ceramic Society

DOI (link to publication from Publisher):
10.1111/jace.18152

Publication date:
2022

Document Version
Accepted author manuscript, peer reviewed version

Impact of network topology on the thermal and mechanical properties of lithium germanate glasses

Søren S. Sørensen[1], *Theany To*[1], *Johan F. S. Christensen*[1], *Hicham Johra*[2], *Morten M. Smedskjaer*[1,*]

[1] Department of Chemistry and Bioscience, Aalborg University, DK-9220 Aalborg, Denmark

[2] Department of the Built Environment, Aalborg University, DK-9220 Aalborg, Denmark

* Corresponding Author. Email: mos@bio.aau.dk

Keywords: Oxide glasses, thermal conductivity, hardness, fracture toughness, lithium germanate, topological constraint theory

Abstract

In this work, we study the structure-topology-property relations of a series of melt-quenched lithium germanate glasses. These glasses exhibit the so-called germanate anomaly, that is, the germanium atoms feature a distribution of four- and higher-coordinated germanium species, manifesting itself as anomalies in several material properties. Here, we couple variations in the number of atomic bond constraints with measured variations in thermal and mechanical properties, including thermal conductivity, Vickers hardness, and fracture toughness. For thermal conductivity, a strong correlation is found with sound velocity as well as with the volumetric constraint density. For hardness, a good correlation with volumetric constraint density is found, whereas, for fracture toughness, variations in network topology alone are insufficient to explain the composition-property relation. To account for this, we apply a recent model which incorporates knowledge of local structure, mechanical properties, and fracture patterns to predict the fracture toughness, showing a good qualitative agreement with the experimental data.

1. Introduction

Germanate glasses are important materials for applications within, e.g., photonics and lasers due to their low losses and large transmission range[1,2] and have also been investigated for sensing applications when doped with lanthanides.[3] The structure of pure germania (GeO_2) resembles that of silica (SiO_2) due to its tetrahedral four-fold coordination in both amorphous and crystalline states, yet it features an anomaly compared to silica when mixed with network modifiers.[4–6] For example, the density of alkali germanates increases with modifier concentration until reaching a maximum value before decreasing.[7] This behavior is similar to the more well-known boron anomaly, involving the coordination number change of boron from three to four in modified borate glass systems.[8,9] The origin of the germanate anomaly is commonly attributed to a transition from four- to five and/or six-fold coordinated germanium (Ge^{IV}, Ge^{V}, and Ge^{VI}, respectively),[10,11] yet significant debate remains regarding which species dominate.[11–13] That is, the germanate anomaly was initially proposed by several authors to be caused by a coordination number shift of Ge from four to six,[7,14] while other authors have later argued that no coordination number change occured in the alkali germanate system and that the anomaly was caused by small ring-type structures.[4,6,15] Other studies based on extended x-ray absorption fine structure as well as x-ray and neutron total scattering methods have provided strong evidence for a coordination number change upon modifier addition.[10,14,16] However, this gave no clear answer to whether a coordination number change to five, six, or both was involved.[10] More recently, Hannon *et al.*[12] have proposed a structural model similar to that for alkali borates, arguing that a five-coordinated state must be the prevalent species. Furthermore, MD simulations have found that either a combination of five- and six-coordinates species or only the latter to be present in a $2Na_2O$-$9GeO_2$ glass based on two potential parameterizations.[17] A structural model based on only four- and six-coordinated Ge has also been proposed as input for a topological constraint model, showing improved agreement with experiments compared to Hannon's model incorporating four- and five-coordinated Ge.[13] Overall, the origin of the anomaly therefore remains to be fully clarified.

In any case, the structural transition in germanate glasses manifests itself as extrema in numerous material properties, including glass transition temperature,[18,19] refractive index,[7] elastic modulus,[20,21]

and sound velocity.[20–23] For alkali germanates, the maximum is typically observed at ~18 mol% alkali oxide,[7] while it approaches 30 mol% in alkaline earth germanates (CaO, SrO, BaO).[11] This non-monotonic property evolution with composition makes the modified germanate system ideal for understanding composition-structure-topology-property relations of glasses.

A common model used to build such relationships is topological constraint theory (TCT). Within this framework, atomic bonds are treated like mechanical trusses – so-called bond constraints. Each atom is then given a certain amount of constraints based on its number of rigid bonds and rigid bond angles. Weighing the number of constraints per atom (n_c) against the degrees of freedom of the atoms (an atom in a three-dimensional system has three degrees of freedom) provides a description of the mechanical flexibility of the system.[24] Formally, when $n_c<3$, the system is termed as underconstrained, when $n_c>3$ the system is overconstrained, and finally when $n_c=3$, the system is said to be isostatic. Underconstrained structures will generally show a lack of resistance to deformation, while overconstrained structures will be rigid yet stressed. Consequently, the isostatic condition will provide rigid, yet stress-free structures. TCT has been applied to several glass families including chalcogenides,[25] borates,[26] phosphates,[27] borophosphates,[28] borosilicates,[29] phosphosilicates[30], and even metal-organic framework glasses,[31] with reported correlations between the number of constraints and multiple glass properties, such as hardness,[32] elastic moduli,[33,34] and liquid fragility[26]. As mentioned above, a TCT model has recently been proposed by Welch *et al.* for the alkali germanate system that enables an accurate prediction of the glass transition temperature, liquid fragility, and Young's modulus for a few selected alkali germanate glasses.[13] Other properties which have previously been linked with network topology, yet remain untested for germanates, include hardness[32], thermal conductivity,[35,36] and fracture toughness.[37]

In this work, we test this recently developed constraint model for alkali germanates of Welch *et al.*[13] using their underlying structural model (assuming only Ge^{IV} and Ge^{VI} species) based on statistical mechanics. This is done in an attempt to understand the composition-structure-topology-property relations in the lithium germanate system. To this end, we probe a series of $x$$Li_2O$-(100-$x$)$GeO_2$ glasses with $x \in \{5,10,15,20,25,30\}$, which are known to feature non-monotonic composition scaling

in several physical properties, including density and glass transition temperature.[7,19] Specifically, we choose to focus on three properties, which have previously been linked with topological models, [32,35–37] but have not yet been experimentally measured for this glass series, namely, the glasses' thermal conductivity, hardness, and fracture toughness. Overall our attempt to predict different thermal and mechanical properties of the lithium germanate glasses using the topological model showcases a clear correlation with network rigidity for most, but not all, of the properties.

2. Experimental

2.1 Glass synthesis

Glasses were prepared in the xLi$_2$O-(100-x)GeO$_2$ series using the traditional melt-quench technique. That is, raw materials of GeO$_2$ (Alfa Aesar or Chempur, ≥99.98%) and Li$_2$CO$_3$ (Merck, ≥98.5%) were mixed and melted in a 90Pt-10Rh crucible at 1300-1400°C for 2 hours, before being quenched and pressed between two pieces of brass. The obtained samples were then annealed at their respective glass transition temperature (T_g) for ~30 min and subsequently cut, ground, and polished for each specific analysis (see details below). Due to the hygroscopic nature of the germanate glasses, they were stored in a desiccator when not being handled or tested. The glasses are identified as xLi(100-x)Ge as an abbreviation of the xLi$_2$O-(100-x)GeO$_2$ composition. For example, the 30Li$_2$O-70GeO$_2$ glass will be denoted as 30Li70Ge in the following.

X-ray diffraction experiments on the annealed glasses were performed using a PANalytical Empyrean diffractometer equipped with a Cu Kα (λ=1.5406 Å) source. Samples were ground in a mortar and loaded onto a zero-background plate made of monocrystalline silicon before an X-ray diffractogram was recorded in the range of 2θ from 10° to 70°. All samples were found to be non-crystaline (see Supplemental Materials Figure S1).

2.2 Density

The density of the samples (ρ) was determined using Archimedes' principle of buoyancy in absolute ethanol at room temperature, that is,

$$\rho = \frac{\rho_{\mathrm{EtOH}} m_{\mathrm{air}}}{m_{\mathrm{air}} - m_{\mathrm{sub}}}, \quad (1)$$

where ρ_{EtOH} is the density of absolute ethanol (0.7871 g cm^{-3}), m_{air} is the weight of the sample in air, and m_{sub} is the weight of the sample when submerged in ethanol.

2.3 Differential scanning calorimetry

All differential scanning calorimetry (DSC) measurements were conducted using a Netzsch 449F1 instrument with PtRh crucibles. T_g of each glass was estimated by heating glass samples of ~20-40 mg from room temperature to above T_g at a rate of 10 K min^{-1}. The temperature was then decreased to below T_g with a cooling rate of 10 K min^{-1}, before reheating to above T_g at 10 K min^{-1}. Proper initial annealing of the glasses was confirmed by the fact that only minor changes in the T_g upon reheating was observed. We used the onset T_g from the second upscan (i.e., with a well-defined thermal history) for further analyses except in the case of the 5Li95Ge glass, which showed two glass transitions in its second upscan, likely due to a minor degree of phase separation upon the first upscan. The possibility of phase separation of GeO_2-rich lithium germanate glasses has previously been discussed,[38] but all the present glasses appeared transparent and with no visual signs of phase separation upon quenching and subsequent annealing.

Next, the determination of isobaric heat capacities (C_p) at room temperature was conducted as this data is needed to convert thermal diffusivity to thermal conductivity (see below). These measurements were done using flat cylindrical samples of ~20-30 mg, which were polished to an optical finish prior to measurements. The measurements were corrected using sapphire crystal as the calibration material. Heat capacities were fitted from ~150 °C to ~50 °C below T_g using the Maier-Kelley equation,[39]

$$C_p(T) = a + bT - cT^{-2}, \quad (2)$$

where a, b, and c are fitting parameters and T is temperature. This fitting was used to extrapolate C_p to room temperature.

2.4 Laser flash analysis

Thermal diffusivity (α) at 300 K was measured using laser flash analysis (Netzsch LFA 447, equipped with a Xenon flash lamp). Samples were cylinders of Ø~5.5 mm and thicknesses in the range of 0.8-1.5 mm, all polished to an optical finish. The variation in thickness was typically within ±10 μm across the surface plane. Prior to the measurements, samples were coated with a thin layer of graphite to ensure complete absorption of the laser pulse and adequate surface temperature measurement with an infrared sensor. The time-dependent temperature rise caused by the laser pulse was then fitted to a numerical model from which α was determined.[40] The reported values of α are averages of at least 10 measurements and are presented in Table 2 and Supplemental Materials Figure S2. From the estimated C_p, ρ, and α data, we calculated thermal conductivity (κ) as,

$$\kappa = C_p \rho \alpha. \quad (3)$$

2.5 Vickers hardness testing

Vickers hardness (H_V) of the studied glasses was measured on samples polished to an optical finish using 3 μm anhydrous diamond suspensions. Using a Struers Duramin-40 indenter equipped with a Vickers diamond tip, each glass was subjected to indentation using a maximum load (P) of 0.196 N (20 gf) and a dwell time of 10 s at ambient conditions (~22 °C, 15-35% relative humidity). This load was sufficiently low to avoid any cracking. H_V was then determined by measuring the diagonal lengths of the impressions (d) and inserting in,

$$H_V = \frac{1.8544P}{d^2}. \quad (4)$$

The reported values of H_V are averages of 10 impressions.

2.6 Single-edge precracked beam fracture toughness

We used the single-edge precracked beam (SEPB) method to determine fracture toughness (K_{Ic}). While originally being an ASTM standard method for ceramics,[41] the method has also been found to be well-suited for determining K_{Ic} of glasses,[42] including small-sized samples (down to ~0.4×0.8×10 mm^3, which is below the ASTM recommendation of lengths, i.e., ≥20 mm).[41,43,44] In detail, the present germanate samples were cut, ground, and polished into beams of typical size ~0.8×1.0×10 mm^3. The samples were ground in ethanol using SiC grinding paper and finally polished to an optical surface finish using a 3 μm anhydrous diamond suspension. Next, a line of three 9.81 N Vickers indents (dwell time of 10 s and separated by ~0.2 mm) were placed across the ~0.8 mm wide face to provide a guide for producing a well-defined precrack. Then, the indented samples were placed in a bridge compression fixture to produce a precrack, extending approximately halfway through the sample. Finally, a three-point bending setup was then used to fracture the pre-cracked samples, with K_{Ic} calculated by,[42]

$$K_{Ic} = \frac{P_{max}}{B\sqrt{W}} Y^*, \quad (5)$$

where Y^* is defined by,

$$Y^* = \frac{3S\beta^{\frac{1}{2}}}{2W(1-\beta)^{\frac{3}{2}}} f(\beta). \quad (6)$$

Here, P_{max} is the maximum load during fracture, W is the width of the sample, B is the sample breadth (the smallest dimension), S is the three-point bending support span (8 mm), β is the ratio of the precrack length to the sample width (a/W), and $f(\beta) = [1.99–(\beta–\beta^2)(2.15–3.93\beta + 2.7\beta^2)]/(1 + 2\beta)$. The average K_{Ic} value was calculated from at least two valid tests.

3. Results and discussion

The germanate anomaly manifests itself in a number of different properties for the lithium germanate system. For example, this is evident in the measured density (ρ) as presented in Figure 1A, showing a good agreement with previously published results for the same glass series.[19] The observed compositional scaling is in strong contrast to that of, e.g., lithium silicates, which show a monotonic change of ρ with increasing Li_2O content in the similar concentration range as the studied lithium germanates.[45] Comparing the variation in density with that in the calculated total number of constraints per atom (n_c),[13] an apparent correlation between ρ and n_c is observed (Figure 1B, see left axis). This is ascribed to the non-monotonic change of the Ge coordination number from four to six (and/or five) when increasing the Li_2O content from x = 0 to ~18 mol% Li_2O and the following reverse transition when x>18 mol% Li_2O.

While n_c has previously been found to govern a variety of glass properties, e.g., T_g and Vickers hardness,[13,32] another interesting metric is the volume normalized number of atomic constraints, the so-called volumetric constraint density (n_c'). To estimate n_c', we follow the procedure as introduced in earlier works[46,47], where the average molar masses (M) of each glass composition is first calculated as,

$$M = \sum_{i=1}^{n} x_i M_i, \quad (7)$$

where M_i is the molar mass of component i with molar fraction of x_i. From Eq. (7) and the value of n_c, the volumetric constraint density (n_c') is calculated as,

$$n_c' = \frac{n_c \rho N_A}{M}, \quad (8)$$

where ρ is the density and N_A is Avogadro's number. The number of atomic constraints and volumetric constraint densities are presented in Table 1. Here, we calculated n_c' specifically for the studied $x$$Li_2O$-(100-$x$)$GeO_2$ system (Figure 1B, right axis, black points), noting that the increase in Li_2O content corresponds to the maximum of n_c' (peak at ~23 mol% Li_2O) and not of n_c. Furthermore,

n_c' reaches an approximately constant value and only shows a minor decrease upon increasing the concentration of Li_2O above 25 mol%.

Next, we consider the thermal properties and first the variation in T_g. Similarly to the compositional scaling of density, T_g shows a non-monotonic variation with a maximum at ~18 mol% Li_2O (Figure 2), suggesting a correlation with n_c as also reported before,[13] where an even better agreement between T_g and n_c was found for rubidium germanate glasses.[13,18] In previous studies, a sharp drop in T_g for alkali germanate glasses of low modifier content has been observed, but this is usually observed at around 1-3 mol% modifier content[19]. Therefore, it is not observed in the present glass series, for which the smallest Li_2O content is 5 mol%.

Notably, other properties feature a different composition dependence compared to density and T_g. For example, the longitudinal (v_L), transversal (v_T), and average (v_s=(v_L+2v_T)/3) speed of sound show a monotonic increase upon increasing Li_2O content in the studied glasses (Figure 3).[23]

As seen in Figure 3, speed of sound exhibits a modest increase with lithium content in the studied compositional region, with no decrease observed in the high-Li_2O compositions as otherwise observed above for density (Figure 1) and T_g (Figure 2). We note that other alkali (e.g., Na, K) germanate glasses feature a pronounced maximum in their speed of sound.[20,22] For the alkali borate system, another oxide glass system featuring a coordination number transition, the speed of sound generally monotonically increases when incorporating light alkali ions (Li, Na), but exhibits a pronounced maximum when introducing heavy alkali ions (K, Rb, Cs).[48] This non-monotonic compositional scaling, observed for both borate and germanate systems, most likely arises from two competiting effects on the speed of sound, namely structure and composition. That is, structure will result in an anomalous behavior of first increasing and then decreasing sound speed due to the related changes in network rigidity (Fig. 1B). In contrast, the continuously changing composition will induce a monotonic change of the sound speed – generally increasing if adding light atoms and decreasing for heavy atoms. This is related to how decreasing atomic mass will impose higher sound speeds for constant bond strength,[49] in good agreement with the plateau region observed in the lithium germanate

(Fig. 3) and lithium borate systems, while significant maxima are found for glasses with heavier modifier ions.[20,22,23]

Similarly to the variation in speed of sound, thermal conductivity (κ) also shows an initial increase with increasing lithium content before reaching a plateau value when approaching 20-25 mol% Li_2O, and a slight further increase for the 30Li70Ge glass (Figure 4A). The observed range of κ values for the lithium germanate glasses is in good agreement with that observed for other alkali oxide glass systems.[47,50] In Figure 4B the correlation between the measured κ and the average speed of sound ($v_s = (2v_T+v_L)/3$) is presented, showing a strong positive correlation for the present germanate glasses as well as for other silicate and borate glass systems.[47,51] Notably, the correlation for the lithium germanates is seen to overlap with that for silicate glasses (Figure 4B).

To gain a deeper understanding of the heat conduction in the germanate glasses, we apply the approach of Allen and Feldman that divides modal types into three categories, namely propagons, diffusons, and locons.[58,59] Propagons are regarded as collective uniform vibrations of periodic eigenvectors, resembling that of the common phonon-picture. These are the dominant heat carriers for most defect-free electrically insulating crystals. In contrast, locons resemble localized vibrations, consisting of only atomic clusters or interfaces, and these are generally believed to contribute little or nothing to heat conduction. Finally, diffusons are, like propagons, collective vibrations, yet of non-periodic (or "diffusive") eigenvectors, providing a weaker contribution than propagons to heat conduction. Generally, the measured thermal conductivity (κ) will thus be a result of contributions from propagons and diffusons, i.e., $\kappa=\kappa_{prop}+\kappa_{diff}$. While the theory of Allen and Feldman involves a direct way to estimate the diffuson contribution to thermal conductivity, it requires the knowledge of atomic position and forces. In contrast, more simple models exist. Cahill, Watson, and Pohl pioneered the area when suggesting a lower limit to thermal conductivity,[60] ultimately resembling the diffuson contribution to thermal conductivity (κ_{diff}). In a similar fashion, Agne *et al.*[61] recently proposed an even simpler description of κ_{diff}, by showing how the temperature dependence of κ_{diff} may be described by,

$$\kappa_{\mathrm{diff}}(T) \approx \frac{n_0^{-\frac{2}{3}} k_{\mathrm{B}}}{2\pi^3 v_{\mathrm{s}}^3} \left(\frac{k_{\mathrm{B}}T}{\hbar}\right)^4 \int_0^{0.95\theta_{\mathrm{D}}T^{-1}} \frac{x^5 \mathrm{e}^x}{(\mathrm{e}^x-1)^2} \mathrm{d}x. \quad (9)$$

Here T denotes temperature, n_0 is atomic number density, k_{B} is the Boltzmann constant, $v_{\mathrm{s}}=(v_{\mathrm{L}}+2v_{\mathrm{T}})/3$ is the average speed of sound, $\hbar = h(2\pi)^{-1}$ is the reduced Planck constant, θ_{D} is the Debye temperature, and $x = \hbar\omega(k_{\mathrm{B}}T)^{-1}$ where ω is the frequency. We estimate θ_{D} as $\theta_{\mathrm{D}} = \hbar(6\pi^2 n_0)^{\frac{1}{3}} v_s k_{\mathrm{B}}^{-1}$ following Ref.[61] Applying Eq. (9) to the studied lithium germanate glasses gives rise to a general increase in κ_{diff} with increasing Li_2O content, with a plateau emerging at 25-30 mol% Li_2O (Figure 4A). Calculating κ_{diff} allows us to indirectly estimate κ_{prop} as $\kappa_{\mathrm{prop}}=\kappa-\kappa_{\mathrm{diff}}$. In our previous work,[35] we observed a relationship between κ_{prop} and volumetric constraint density (n_{c}'). Here, we observe a good correlation between κ and n_{c}' (Figure 5A) and further try to extend the previously reported data of κ_{prop} vs n_{c}' for alkali borates, alkali silicates, and soda lime borosilicates, with the studied lithium germanates (Figure 5B).

Depending on the glass system, different trends in the data are observed in Figure 5B. While the alkali borate system features only a minor change of κ_{prop} with n_{c}', the alkali silicate, borosilicate, and the present lithium germanate glasses all feature increasing κ_{prop} upon increasing n_{c}'. These differences between different glass series may be explained by their differences in atomic constraints, with the alkali borate system generally featuring the lowest number of constraints per atom (n_{c}~3.2), while the other glass series have higher n_{c} values. Tuning n_{c} has previously been shown to enable tuning of, e.g., the presence of locons and hence affect the other modal types and consequently the value of κ.[36,62] Also notably, thermal conductivity has previously been shown to plateau when decreasing the network connectivity to below n_{c}=3 for several systems as also suggested in one of the first papers on TCT by Thorpe.[63,64] Qualitatively, this would thus explain the lower slope in Figure 5B for the borate glasses compared to the other systems.

To further study the composition-structure-topology-property relations in the lithium germanate glasses, we next consider the elastic properties of the system. Using the sound speeds measured by Kaneda *et al.*,[23] the Young's, shear, and bulk moduli (E, G, B, respectively) and Poisson's ratio (ν) of

the glasses were calculated according to Ref.[65] Sound speeds are presented in Table 2, while the calculated elastic constants are presented in Table 3. *E*, *G*, and *B* are presented in Figure 6. All three moduli show the same tendency, i.e., initially an increase with increasing lithium oxide content and then a constant value around the 25Li75Ge and 30Li70Ge glasses. This is similar to what was observed for the speed of sound (Fig. 3) as well as the thermal conductivity (Fig. 4), providing a coupling of mechanical and thermal properties in the probed systems. Comparing the calculated moduli to those of other alkali germanates, the present results for lithium glasses are higher than those of higher atomic mass (e.g., Na and K germanates)[66], which is in agreement with the expected increase of bond strength upon increasing cationic field strength.[67] Generally, the presented values of moduli are within the expected range of oxide glasses.[68]

Next, we consider the compositional variation in hardness, a measure of the resistance to permanent deformation of the glasses. We used a four-sided pyramidal diamond tip with an included angle of 136° between two opposite faces (so-called Vickers tip) to make impressions in the glasses. The impression diagonal length (*d*) is then used to calculate Vickers hardness (H_V) through Eq. (4). The obtained values of H_V for the lithium germanate glasses are presented in Figure 7A.

The hardness of the studied lithium germanate glasses is first found to increase linearly with increasing lithium concentration from the 5Li95Ge (~5.3 GPa) to the 15Li85Ge glass (~7.5 GPa), before showing a small increase to the 20Li80Ge glass and finally a decrease in H_V for the two glasses of highest Li content. This compositional trend is similar to that observed for T_g (Figure 2) and shows the same tendency as the introduced atomic constraints (Figure 1B) with a maximum between 15 and 20 mol% Li_2O. The direct agreement between the number of atomic constraints and H_V fits with the results of previous works on borates.[32] Notably, like thermal conductivity, hardness has previously been suggested to correlate with volumetric constraint density.[46] In Figure 7B, we have plotted H_V as a function of n_c' for the studied lithium germanates as well as for two series of borosilicate and phosphosilicate glasses from the literature.[46] Interestingly, the data for the lithium germanate glasses follow the same trendline as the phosphosilicates, while the borosilicate glasses occupy a separate region of the plot. Fitting a linear function to the presented data while enforcing $H_V(n_c'=0) = 0$ gives

the correlation $H_V(n_c') = 0.068$ GPa·n_c', which is in good agreement with that reported for phosposilicate glasses[46] using similar constraints, namely $H_V(n_c') = 0.06$ GPa·n_c'. The tendency of the germanates to follow the same trend as the phosphosilicates is interesting given how both glass families feature the same variation in coordination numbers. That is, as mentioned the germanates are assumed to contain both Ge^{IV} as well as Ge^{VI} units, while the phosphosilicates feature four-fold coordinated phosphate units as well as a distribution of Si^{IV} and Si^{VI}.[69,70] Considering the similarity of coordination numbers in the germanates and phosphosilicates, their overlapping curve of H_V vs. n_c' in Figure 7B is intriguing.

Lastly, we study the fracture behavior of the glasses by considering the variation in fracture toughness (K_{Ic}), i.e., the ability of the glass to withstand propagation of a pre-existing crack. K_{Ic} has previously been linked with atomic constraints in simulation studies,[37] but has not seen such comparisons in experiments. We determined fracture toughness K_{Ic} through a small-sample single-edge precracked beam (SEPB) method, which has previously been validated for other glassy systems,[43,44] to obtain self-consistent values of K_{Ic}. We will refer to these values as K_{Ic}. Figure 8A shows an example of a fractured 25Li75Ge glass sample from SEPB measurements, demonstrating the presence of a precrack that has grown from the initial indents. We note that it was not possible to prepare samples of adequate size for SEPB measurements for the 30Li70Ge glass due to its tendency to crystallize.

The values of K_{Ic} reported in Figure 8B are found to be in the same range as those of other oxide glass systems including borate and silicate systems (typically 0.5-1.0 MPa $m^{0.5}$).[71] Specifically, K_{Ic} values from SEPB of the lithium germanates are in the range of 0.7-0.9 MPa $m^{0.5}$, with a maximum value for the 15Li85Ge glass. The overall compositional trend in K_{Ic} qualitatively agrees with the variation in atomic constraints (Figure 1B), yet K_{Ic} shows a shifted maximum towards lower Li_2O content

compared to n_c. The observed maximum in the K_{Ic} at around x≈15 mol% Li_2O agrees with previous non-monotonic K_{Ic} data for $x$$Na_2O$-(100-$x$)$GeO_2$ glasses, but the lithium germanates feature lower K_{Ic} than sodium germanates (up to ~1.3 MPa $m^{0.5}$) as measured by the single-edge notched beam (SENB) and double cleavage drilled compression (DCDC) techniques[72,73] as well as a shift towards higher modifier content at maximum K_{Ic}. We note that both the SENB and DCDC methods have been reported to overestimate the fracture toughness values due to large crack tip stress (for SENB) and T-stress (for DCDC).[74,75]

To understand the atomic mechanism of crack propagation in the germanate glasses, we apply a recently developed model of brittle fracture to estimate the composition dependence of fracture toughness.[71] The model relies on estimating K_{Ic} from the measured E and ν values and an estimated value of the fracture surface energy by means of the similarity principle,[76]

$$K_{\mathrm{Ic}}^{\mathrm{Prediction}} = \sqrt{2\gamma^{\mathrm{t}}E'}, \qquad (10)$$

where $E' = E/(1-\nu^2)$ for plane strain and $\gamma^{t} = 0.5(\rho M^{-1})^{2/3}N_A^{-1/3}\sum x_i n_i U_i$ is the theoretical fracture surface energy predicted based on the experimental density (ρ), the average molar mass of the glass (M), and Avogadro's number (N_A). x is the stoichiometry of species involved in the interatomic bond energy (U), and n is the number of required bonds to be broken for the crack to proceed to the next structural unit (note that we consider only the presence of Ge^{IV} and Ge^{VI} species, as also done in the discussed topological model[13]). To this end, we assume that the crack follows the least energy-intensive path. That is, in all cases we assume that the crack will break all ionic Li-O bonds. Next, we assume that the crack will be allowed to propagate when all Ge atoms in the fracture plane reach a coordination number of three. Specifically this implies that between zero and three Ge-O bonds will break in the tetra- or octahedra (depending on the Li_2O concentration) before the crack will grow. The fraction of six-coordinated to total Ge (N_6) was taken from the model of Welch *et al.*[13] (and are presented in Table 3), while diatomic bond energies of 340 and 658 kJ mol^{-1} were used for Li-O and Ge-O, respectively.[77] Using these parameters, we first predicted γ^{t} and then used Eq. (10) to calculate

$K_{Ic}^{Prediction}$. We note that in earlier work,[71] the use of bond energies from Ref.[77] was found to be superior in predicting K_{Ic} compared to the use of other bond energy estimations.

Predicted values of fracture toughness ($K_{Ic}^{Prediction}$) are presented in Figure 8B. $K_{Ic}^{Prediction}$ is generally lower than the K_{Ic} data obtained from SEPB, but, more importantly, the model is shown to correctly capture the initially increasing K_{Ic}, the following maximum at the 15Li85Ge glass, and the subsequent decrease of K_{Ic} when increasing the Li_2O content further. This is notable, given the lack of any straightforward correlation between K_{Ic} and the number of atomic constraints nor the volumetric constraint density (Supplemental Materials Figure S3). The only other studied alkali germanate in terms of K_{Ic}, namely the sodium germanate system, shows a pronounced maximum of K_{Ic} at 10 mol% Na_2O.[72,73] Using data from the literature,[19,20] we make fracture toughness calculations for the sodium germanate system using the same model[71] as for lithium germanates (Supplemental Materials Figure S4). The model suggests a slight shift towards having a maximum for K_{Ic} at lower modifier content. This is in good agreement with the experimental direction of change from Li to Na, yet the model points to a maximum in K_{Ic} between 10 and 15 mol% for the sodium germanates while the experimental data[72,73] suggest a clear maximum around 10 mol% Na_2O.

In the following, we explore the shifting of the K_{Ic} maximum away from the composition with maximum number of constraints (Fig. 1B). First, by estimating the fracture surface energy (γ^i) from the model of Rouxel[71], we find that γ^i exhibits a maximum value at low modifier content (5 mol%) for both NaGe and LiGe glasses (Supplemental Materials Figure S5A), with a more pronounced drop of γ^i for the NaGe glasses. The latter is likely, at least partially, due to the maximum in density for the NaGe at 15 mol% Na_2O compared to that at ~20 mol% Li_2O for the LiGe glasses (Supplemental Materials Figure S5B). As such, we infer that γ^i is the main cause of the shift of K_{Ic} away from the composition with maximum number of constraints. Moreover, the difference in predicted maximum between K_{Ic} of NaGe and LiGe may also be caused by differences in the compositional evolution of Young's modulus for the two glass series. That is, while E mainly increases upon increasing Li_2O content in LiGe Glasses, E exhibits a rather sharp maximum at around 15 mol% Na_2O in NaGe

glasses (Supplemental Materials Figure S5C), ultimately shifting the composition with maximum K_{Ic} towards lower modifier content.

Next, we note that the fracture toughness model greatly underpredicts the experimental values of the sodium germanates, but this may again be related to the overestimation of experimental values. The general underestimation of the absolute values of K_{Ic} by the model may be due to the assumption of a fully brittle fracture. Given two (or three) accessible coordination states and the presence of higher than four-coordinated Ge species in all samples, so-called bond switching events, which have been shown to govern fracture in various glass systems,[43,78–80] may play a role in the fracture process, inducing some nanoscale ductility. That is, when applying strain on a structure, the multiple occupied and accessible coordination states will allow for significant atomic rearrangement before fracture is obtained, hence representing a plastic fracture process. As an example, the Ge^{VI} atoms may rearrange under an applied strain to decrease the local stress they experience, resulting in a change of the coordination state to Ge^{IV} prior to undergoing crack propagation. Similarly, an increase in coordination number or bond swapping (where coordination number increases again after decreasing) may play a role in the observed disagreement in the absolute values of K_{Ic}.

4. Conclusions

In summary, we have investigated the thermal and mechanical properties of six lithium germanate glasses, including thermal conductivity, hardness, and fracture toughness. We find these three properties to feature pronounced germanate anomaly behavior, i.e., the composition-property correlation shows a maximum upon increasing Li_2O content. Based on a recent topological model of the alkali germanate system, we find good correlations between network topology and both thermal conductivity and hardness, in good agreement with earlier studies on oxide glasses. However, the topological model is inadequate in predicting the composition dependence of fracture toughness in the lithium germanate glasses. Instead, a model based on mechanical properties, individual bond energies, and assumptions on fracture behavior is needed to accurately predict the composition dependence of

fracture toughness. This work sheds light on how network topology affects various properties in the alkali germanate glass series, ultimately aiding the development of predictive composition-structure-property models in a broad family of oxide glasses.

Acknowledgments

This work was supported by the Independent Research Fund Denmark (grant no. 7017-00019). We thank M. L. Bødker (Aalborg University) and R. S. Welch (Pennsylvania State University) for helpful discussions regarding the topological model.

Notes

The authors declare no competing interests.

REFERENCES

1. Munasinghe HT, Winterstein-Beckmann A, Schiele C, *et al.* Lead-germanate glasses and fibers: a practical alternative to tellurite for nonlinear fiber applications. *Opt Mater Express*. 2013;3(9):1488.

2. Wen X, Tang G, Yang Q, *et al.* Highly Tm^{3+} doped germanate glass and its single mode fiber for 2.0 μm laser. *Sci Rep*. 2016;6:20344.

3. Pisarski WA, Pisarska J, Lisiecki R, Ryba-Romanowski W. Er^{3+}/Yb^{3+} co-doped lead germanate glasses for up-conversion luminescence temperature sensors. *Sensors Actuators, A Phys*. 2016;252:54–58.

4. Henderson GS, Fleet ME. The structure of glasses along the Na_2O-GeO_2 join. *J Non Cryst Solids*. 1991;134(3):259–269.

5. Micoulaut M, Cormier L, Henderson GS. The structure of amorphous, crystalline and liquid GeO_2. *J Phys Condens Matter*. 2006;18:R753.

6. Henderson GS, Wang HM. Germanium coordination and the germanate anomaly. *Eur J Mineral*. 2002;14(4):733–744.

7. Murthy MK, Ip. J. Some Physical Properties of Alkali Germanate Glasses. *Nature*. 1964;201:285–286.

8. Uhlmann DR, Shaw RR. The Thermal Expansion of Alkali Borate Glasses and the Boric Oxide Anomaly. *J Non Cryst Solids*. 1969;1:347–359.

9. Feller SA, Dell WJ, Bray PJ. ^{10}B NMR studies of lithium borate glasses. *J Non Cryst Solids*. 1982;51:21–30.

10. Hoppe U, Kranold R, Weber HJ, Hannon AC. Change of the Ge-O coordination number in potassium germanate glasses probed by neutron diffraction with high real-space resolution. *J*

Non Cryst Solids. 1999;248(1):1–10.

11. Alderman OLG, Hannon AC, Feller S, Beanland R, Holland D. The Germanate Anomaly in Alkaline Earth Germanate Glasses. *J Phys Chem C*. 2017;121(17):9462–9479.

12. Hannon AC, Di Martino D, Santos LF, Almeida RM. A model for the Ge-O coordination in germanate glasses. *J Non Cryst Solids*. 2007;353(18–21):1688–1694.

13. Welch RS, Wilkinson CJ, Shih YT, *et al.* Topological model of alkali germanate glasses and exploration of the germanate anomaly. *J Am Ceram Soc*. 2020;103:4224–4233.

14. Sakka S, Kamya K. Structure of Alkali Germanate Glasses Studied by Spectroscopic Techniques. *J Non Cryst Solids*. 1982;49:103–116.

15. Wang HM, Henderson GS. The germanate anomaly: Is the presence of five- or six-fold Ge important? *Phys Chem Glas*. 2005;46(4):377–380.

16. Huang WC, Jain H, Marcus MA. Structural study of Rb and (Rb, Ag) germanate glasses by EXAFS and XPS. *J Non Cryst Solids*. 1994;180:40–50.

17. Nanba T, Kieffer J, Miura Y. Molecular dynamic simulation on the structure of sodium germanate glasses. *J Non Cryst Solids*. 2000;277(2–3):188–206.

18. Kiczenski TJ, Ma C, Hammarsten E, Wilkerson D, Affatigato M, Feller S. Study of selected physical properties of alkali germanate glasses over wide ranges of composition. *J Non Cryst Solids*. 2000;272(1):57–66.

19. Ashton-Patton MM. PROPERTIES OF MIXED ALKALI GERMANATE GLASSES. Alfred University; 2013

20. Shaw RR. Sonic Velocities, Elastic Properties, and Microhardness of Sodium Germanate Glasses. *J Am Ceram Soc*. 1971;54(3):170–171.

21. Sapian IN, Hisam R, Yahya AK, Yusof MIM. The influence of germanate anomaly on elastic moduli and Debye temperature behavior of xLi2O-(100 − x)[0.65GeO2·0.35PbO] glass system. *J Non Cryst Solids*. 2018;493:99–107.

22. Mamiya S, Matsuda Y, Kaneda K, Kawashima M, Kojima S. Brillouin scattering study of binary potassium germanate glasses. *Mater Sci Eng B*. 2010;173:155–157.

23. Kaneda K, Matsuda Y, Kojima S. Elastic properties of lithium germanate glasses studied by Brillouin scattering. *Jpn J Appl Phys*. 2010;49:07HB03.

24. Mauro JC. Topological constraint theory of glass. *Am Ceram Soc Bull*. 2011;90(4):31–37.

25. Wang Y, Boolchand P, Micoulaut M. Glass structure, rigidity transitions and the intermediate phase in the Ge-As-Se ternary. *Europhys Lett*. 2000;52(6):633–639.

26. Mauro JC, Gupta PK, Loucks RJ. Composition dependence of glass transition temperature and fragility. II. A topological model of alkali borate liquids. *J Chem Phys*. 2009;130:234503.

27. Hermansen C, Rodrigues BP, Wondraczek L, Yue Y. An extended topological model for binary phosphate glasses. *J Chem Phys*. 2014;141:244502.

28. Hermansen C, Youngman RE, Wang J, Yue Y. Structural and topological aspects of borophosphate glasses and their relation to physical properties. *J Chem Phys*. 2015;142:184503.

29. Smedskjaer MM, Mauro JC, Youngman RE, Hogue CL, Potuzak M, Yue Y. Topological principles of borosilicate glass chemistry. *J Phys Chem B*. 2011;115(44):12930–12946.

30. Hermansen C, Guo X, Youngman RE, Mauro JC, Smedskjaer MM, Yue Y. Structure-topology-property correlations of sodium phosphosilicate glasses. *J Chem Phys*. 2015;143:064510.

31. Yang Y, Wilkinson CJ, Lee KH, *et al.* Prediction of the Glass Transition Temperatures of

Zeolitic Imidazolate Glasses through Topological Constraint Theory. *J Phys Chem Lett*. 2018;9(24):6985–6990.

32. Smedskjaer MM, Mauro JC, Yue Y. Prediction of glass hardness using temperature-dependent constraint theory. *Phys Rev Lett*. 2010;105:115503.

33. Yang K, Yang B, Xu X, Hoover C, Smedskjaer MM, Bauchy M. Prediction of the Young's modulus of silicate glasses by topological constraint theory. *J Non Cryst Solids*. 2019;514:15–19.

34. Wilkinson CJ, Zheng Q, Huang L, Mauro JC. Topological constraint model for the elasticity of glass-forming systems. *J Non-Crystalline Solids X*. 2019;2:100019.

35. Sørensen SS, Bødker MS, Johra H, *et al.* Thermal conductivity of densified borosilicate glasses. *J Non Cryst Solids*. 2021;557(April):120644.

36. Aryana K, Stewart DA, Gaskins JT, *et al.* Tuning network topology and vibrational mode localization to achieve ultralow thermal conductivity in amorphous chalcogenides. *Nat Commun*. 2021;12:2817.

37. Bauchy M, Wang B, Wang M, *et al.* Fracture toughness anomalies: Viewpoint of topological constraint theory. *Acta Mater*. 2016;121:234–239.

38. Shaw RR, Uhlmann DR. Effect of phase separation on the properties of simple glasses I. Density and molar volume. *J Non Cryst Solids*. 1969;1:474–498.

39. Maier CG, Kelley KK. An equation for the representation of high-temperature heat content data. *J Am Chem Soc*. 1932;54(8):3243–3246.

40. Mehling H, Hautzinger G, Nilsson O, Fricke J, Hofmann R, Hahn O. Thermal diffusivity of semitransparent materials determined by the laser-flash method applying a new analytical model. *Int J Thermophys*. 1998;19(3):941–949.

41. ASTM C1421-10, Standard Test Methods for Determination of Fracture Toughness of Advanced Ceramics at Ambient Temperature, ASTM International, West Conshohocken, PA. 2010.

42. To T, Célarié F, Roux-Langlois C, *et al.* Fracture toughness, fracture energy and slow crack growth of glass as investigated by the Single-Edge Precracked Beam (SEPB) and Chevron-Notched Beam (CNB) methods. *Acta Mater*. 2018;146:1–11.

43. To T, Sørensen SS, Christensen JFS, *et al.* Bond Switching in Densified Oxide Glass Enables Record-High Fracture Toughness. *ACS Appl Mater Interfaces*. 2021;13(15):17753–17765.

44. To T, Sørensen SS, Stepniewska M, *et al.* Fracture toughness of a metal-organic framework glass. *Nat Commun*. 2020;11:2593.

45. Tischendorf B, Ma C, Hammersten E, *et al.* The density of alkali silicate glasses over wide compositional ranges. *J Non Cryst Solids*. 1998;239:197–202.

46. Zheng Q, Yue Y, Mauro JC. Density of topological constraints as a metric for predicting glass hardness. *Appl Phys Lett*. 2017;111:011907.

47. Sørensen SS, Pedersen EJ, Paulsen FK, *et al.* Heat conduction in oxide glasses: Balancing diffusons and propagons by network rigidity. *Appl Phys Lett*. 2020;117:031901.

48. Kodama M, Kojima S. Velocity of Sound in and Elastic Constants of Alkali Metal Borate Glasses. *Phys Chem Glas Eur J Glas Sci Technol Part B*. 2014;55(1):1–12.

49. Kittel C. Introduction to Solid State Physics. 8th ed. Wiley; 2005

50. Choudhary MK, Potter RM. Heat transfer in glass-forming melts. In: Pye LD, Montenero A, Joseph I, eds. *Prop. Glas. Melts*. CRC Press, Taylor and Francis; 2005

51. Hayes DJ, Rea SN, Hilton AR. Thermal Conductivity of Infrared Transparent Chalcogenide Glasses. *J Am Ceram Soc*. 1975;58(3–4):135–137.

52. Ammar MM, Gharib SA, Halawa MM, El-Batal HA, El-Badry K. Thermal Conductivity of Silicate and Borate Glasses. *Commun Am Ceram Soc*. 1983;66(5):C-76-77.

53. Sørensen SS, Johra H, Mauro JC, Bauchy M, Smedskjaer MM. Boron anomaly in the thermal conductivity of lithium borate glasses. *Phys Rev Mater*. 2019;3(7):075601.

54. Lorösch J, Couzi M, Pelous J, Vacher R, Levasseur A. Brillouin and Raman scattering study of borate glasses. *J Non Cryst Solids*. 1984;69:1–25.

55. Hiroshima Y, Hamamoto Y, Yoshida S, Matsuoka J. Thermal conductivity of mixed alkali silicate glasses at low temperature. *J Non Cryst Solids*. 2008;354:341–344.

56. Inaba S, Oda S, Morinaga K. Equation for Estimating the Thermal Diffusivity, Specific Heat and Thermal Conductivity of Oxide Glasses. *J Japan Inst Met*. 2001;65(8):680–687.

57. Khanisanij M, Sidek HAA. Elastic behavior of borate glasses containing lead and bismuth oxides. *Adv Mater Sci Eng*. 2014;2014:452830.

58. Allen PB, Feldman JL. Thermal Conductivity of Glasses: Theory and Application to Amorphous Si. *Phys Rev Lett*. 1989;62(6):645–648.

59. Allen PB, Feldman JL. Thermal conductivity of disordered harmonic solids. *Phys Rev B*. 1993;48(17):12581–12588.

60. Cahill DG, Watson SK, Pohl RO. Lower limit to the thermal conductivity of disordered crystals. *Phys Rev B*. 1992;46(10):6131–6140.

61. Agne MT, Hanus R, Snyder GJ. Minimum thermal conductivity in the context of: Diffuson - mediated thermal transport. *Energy Environ Sci*. 2018;11:609–616.

62. Braun JL, King SW, Giri A, *et al.* Breaking network connectivity leads to ultralow thermal conductivities in fully dense amorphous solids. *Appl Phys Lett*. 2016;109:191905.

63. King SW, Bielefeld J, Xu G, *et al.* Influence of network bond percolation on the thermal, mechanical, electrical and optical properties of high and low-k a-SiC:H thin films. *J Non Cryst Solids*. 2013;379:67–79.

64. Thorpe MF. Continuous deformations in random networks. *J Non Cryst Solids*. 1983;57(3):355–370.

65. Gersten JI, Smith FW. The Physics and Chemistry of Materials. Wiley; 2001

66. Osaka A, Takahashi K, Ariyoshi K. The elastic constant and molar volume of sodium and potassium germanate glasses and the germanate anomaly. *J Non Cryst Solids*. 1985;70:243–252.

67. Dietzel A. Die kationenfeldstärken und ihre beziehungen zu entglasungsvorgängen, zur verbindungsbildung und schmelzpunkten von silikaten. *Z Elektrochem Angew Phys Chem*. 1942;48(1):9–23.

68. Varshneya AK. Fundamentals of inorganic glasses. 2013

69. Dupree R, Holland D, Mortuza MG. Six-coordinated silicon in glasses. *Nature*. 1987;328:416–417.

70. Ren J, Eckert H. Superstructural Units Involving Six-Coordinated Silicon in Sodium Phosphosilicate Glasses Detected by Solid-State NMR Spectroscopy. *J Phys Chem C*. 2018;122(48):27620–27630.

71. Rouxel T. Fracture surface energy and toughness of inorganic glasses. *Scr Mater*. 2017;137:109–113.

72. Vernaz E, Larche F, Zarzycki J. Fracture Toughness-Composition Relationship in Some Binary and Ternary Glass Systems. *J Non Cryst Solids*. 1980;37:359–365.

73. Yoshida S, Matsuoka J, Soga N. Sub-critical crack growth in sodium germanate glasses. *J Non*

Cryst Solids. 2003;316:28–34.

74. Rouxel T, Yoshida S. The fracture toughness of inorganic glasses. *J Am Ceram Soc*. 2017;100:4374–4396.

75. Lacondemine T. Initiation et propagation d'une fissure dans un composite particulaire à matrice verre : expérimentation et analyse numérique. L'UNIVERSITE DE RENNES 1; 2019

76. Irwin GR. Analysis of Stresses and Strains Near the End of a Crack Traversing a Plate. *J Appl Mech*. 1957;24(3):361–364.

77. Lide D. R. CRC handbook of chemistry and physics. 86th ed. n.d.

78. To T, Sørensen SS, Yue Y, Smedskjaer MM. Bond switching is responsible for nanoductility in zeolitic imidazolate framework glasses. *Dalt Trans*. 2021;50(18):6126–6132.

79. Frankberg EJ, Kalikka J, Ferré FG, *et al.* Highly ductile amorphous oxide at room temperature and high strain rate. *Science (80-)*. 2019;366(6467):864–869.

80. Luo J, Wang J, Bitzek E, *et al.* Size-Dependent Brittle-to-Ductile Transition in Silica Glass Nanofibers. *Nano Lett*. 2016;16:105–113.

FIGURE CAPTIONS

Figure 1. (A) Density [ρ] as well as (B) total number of atomic constraints [n_c, left axis] and volumetric constraint density [n_c', right axis] as a function of Li_2O content in the studied xLi_2O-(100-x)GeO_2 system. In (A), literature density data from Ref. [19] are shown for comparison. The red dashed line in (B) indicates the number of topological constraints between the studied compositions [red points] as calculated from the topological constraint model of Welch *et al*.[13] We note how some error bars in (A) and all of the error bars of n_c' in (B) are smaller than the size of the symbols.

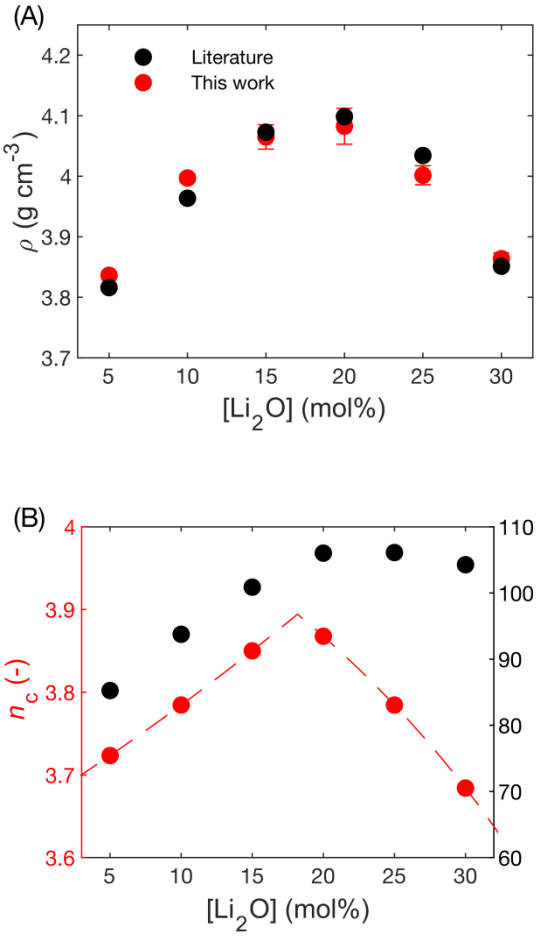

Figure 2. Glass transition temperature (T_g) as a function of Li_2O content in the studied xLi_2O-(100-x)GeO_2 system. The estimated error of T_g is 2 K, i.e., smaller than the size of the symbols.

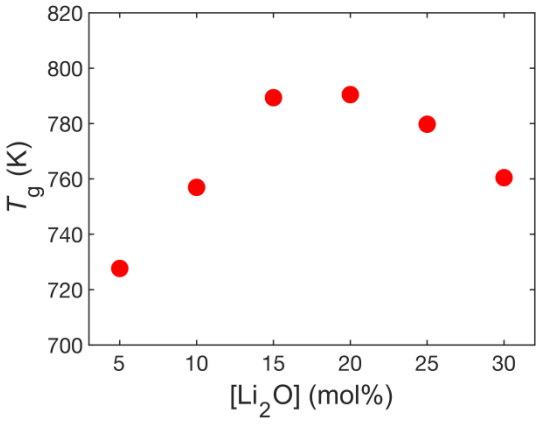

Figure 3. Longitudinal (red), transversal (green), and average (black) sound speeds (v_L; v_T; and v_s = $(2v_T+v_L)/3$, respectively) as a function of Li_2O content in the studied xLi_2O-(100-x)GeO_2 system. The longitudinal and transversal sound speed data is taken from Kaneda *et al.*[23] for the glasses with >5 mol% Li_2O. The values for the $5Li_2O$-$95GeO_2$ glass were extrapolated from other lithium germanate glasses down to a composition of approximately $6Li_2O$-$94GeO_2$ as introduced in Ref.[23]

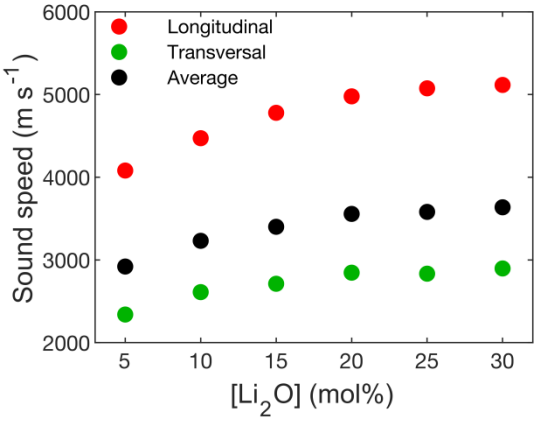

Figure 4. (A) Thermal conductivity [κ] and estimated diffuson contribution to thermal conductivity [κ_{diff}] as a function of Li_2O content in the studied xLi_2O-(100-x)GeO_2 system. (B) Correlation between the average speed of sound [v_s] and κ for the studied glasses as well as a number of silicate [black] and borate [green] glasses from Refs.[47,52–57] Estimated errors are smaller than the size of the symbols. The red dashed line in (B) is a linear fit, serving as a guide for the eye for the germanate data.

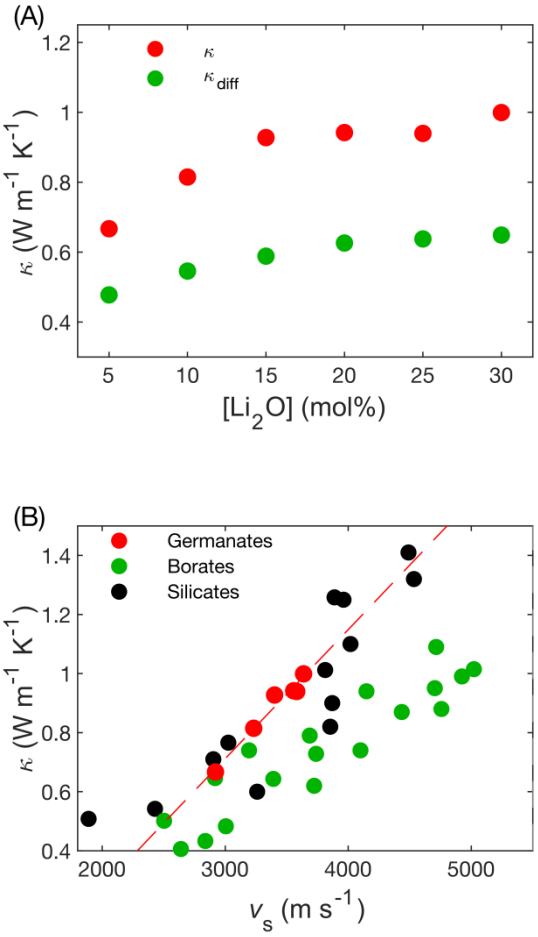

Figure 5. Correlation between (A) volumetric constraint density [n_c'] and measured thermal conductivity [κ] for the studied xLi$_2$O-(100-x)GeO$_2$ glasses as well as between (B) n_c' and the estimated propagon contribution to thermal conductivity [κ_{prop}] for the lithium germanates of this study as well as previously studied borosilicate, alkali silicate, and alkali borate glasses.[35,47,53] Errors in (B) for lithium germanates are all smaller than the size of the symbols.

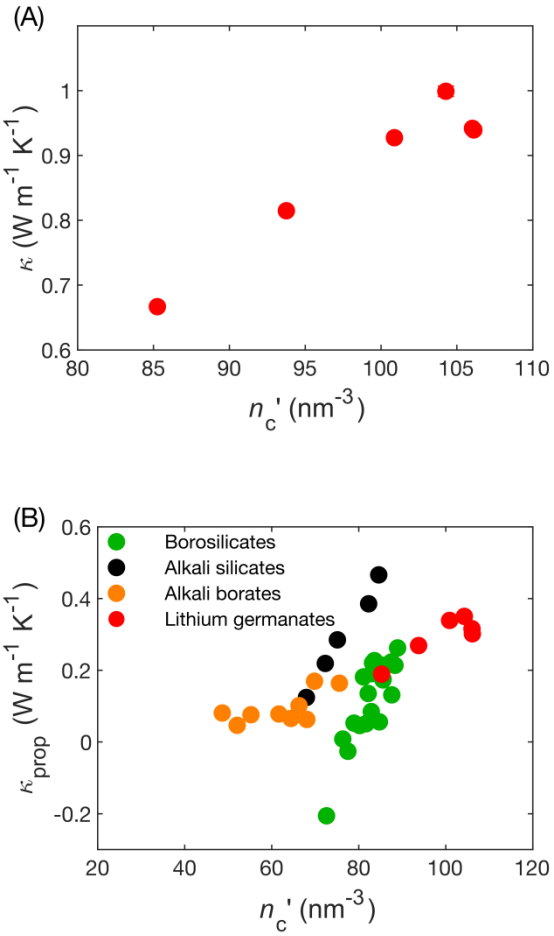

Figure 6. Young's modulus (*E*, red points), shear modulus (*G*, green points), and bulk modulus (*B*, black points) for the studied glasses as a function of Li_2O content. Sound speeds used for calculations of moduli were taken from Kaneda *et al*.[23] Errors are all smaller than the size of the symbols.

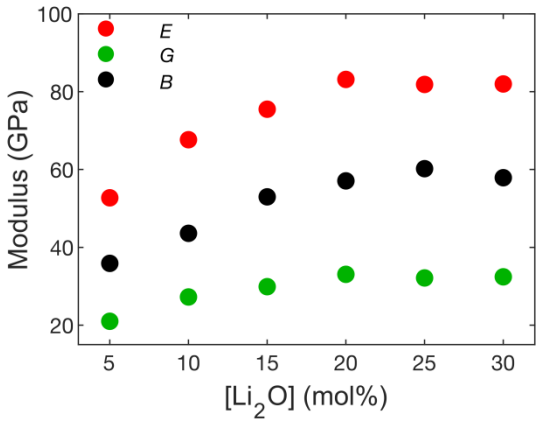

Figure 7. Vickers hardness [H_V] as a function of (A) Li_2O content and (B) volumetric constraint density [n_c']. The correlation between H_V and n_c' for lithium germanate [red points] is compared to that of borosilicate [green points] and phosphosilicate [black points] glasses as reported elsewhere [H_V of boro- and phosposilicates were measured using loads of 0.25 N and 0.49 N, respectively].[46] Error bars in (B) for germanates are sometimes smaller than the size of the symbols and are unreported for the boro- and phosphosilicates taken from literature.

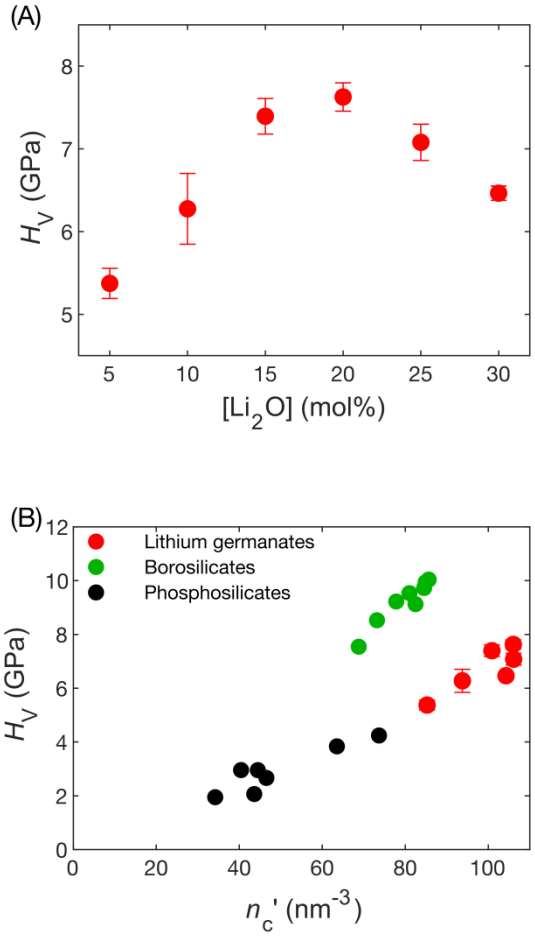

Figure 8. (A) Micrograph of a fractured 25Li75Ge glass sample after the self-consistent single-edge precracked beam [SEPB] measurement, showing the three indents used to make the precrack as well as a clear precrack front. Note that the image was reconstructed by stitching four images together. (B) Fracture toughness determined from SEPB measurements [K_{Ic}] as well as the prediction of fracture toughness [$K_{\mathrm{Ic}}^{\mathrm{Prediction}}$] using the model of Ref.[71] as a function of Li_2O content. We note how the 30Li70Ge glass was too prone to crystallization to obtain samples of adequate sizes for SEPB measurements.

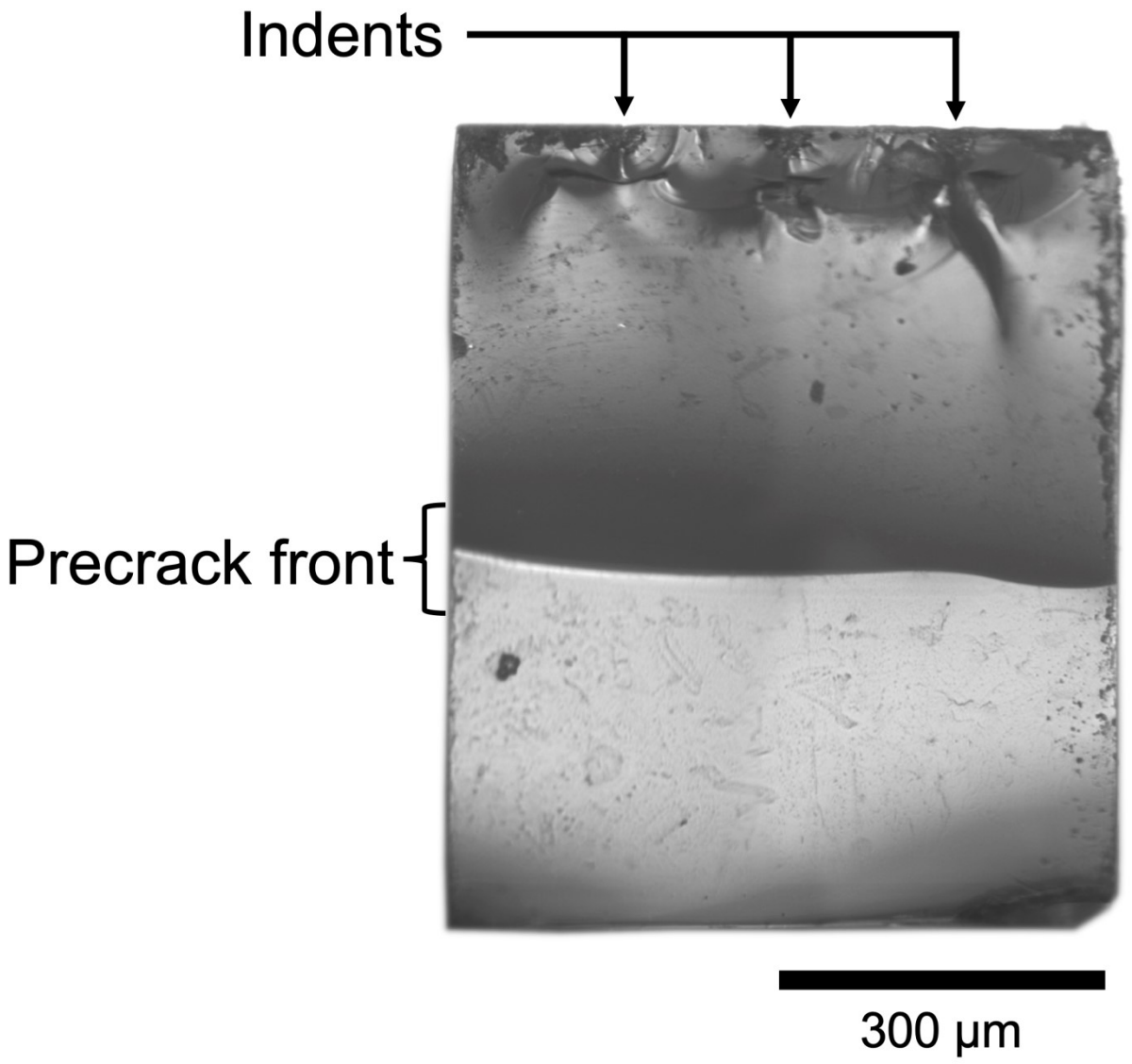

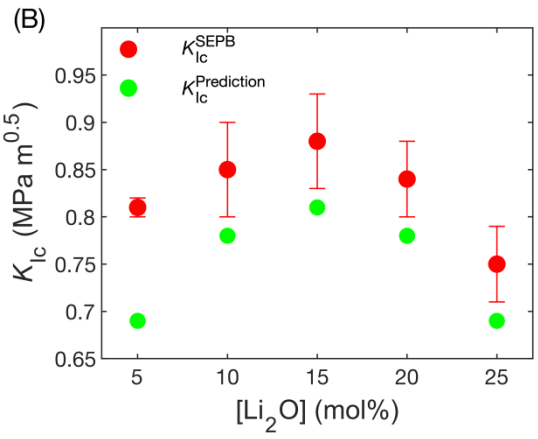

TABLES

Table 1. Density (ρ), glass transition temperature (T_g), total number of atomic constraints per atom (n_c), and volumetric constraint density (n_c') for the prepared lithium germanate glass series. Estimated average errors of ρ, T_g, and n_c' are 0.01 g cm^{-3}, 2 K, and 0.1 nm^{-3}, respectively.

Glass-ID	ρ (g cm^{-3})	T_g (K)	n_c* (-)	n_c' (nm^{-3})
5Li95Ge	3.84	728	3.72	85.3
10Li90Ge	4.00	757	3.78	93.8
15Li85Ge	4.06	789	3.85	100.9
20Li80Ge	4.08	790	3.87	106.0
25Li75Ge	4.00	780	3.78	106.1
30Li70Ge	3.86	760	3.68	104.3

*Data obtained from Ref.[13]

Table 2. Heat capacity (C_p), longitudinal sound speed (v_L), transversal sound speed (v_T), average sound speed ($v_S=(v_L+2v_T)/3$), thermal diffusivity (α), thermal conductivity (κ), and diffuson contribution to thermal conductivity (κ_{diff}) for the prepared lithium germanate glass series. Estimated average errors for α and κ are 0.003 mm^2 s^{-1} and 0.005 W m^{-1} K^{-1}, respectively.

Glass-ID	C_p (J g^{-1} K^{-1})	v_L^* (m s^{-1})	v_T^* (m s^{-1})	v_s (m s^{-1})	α (mm^2 s^{-1})	κ (W m^{-1} K^{-1})	κ_{diff} (W m^{-1} K^{-1})
5Li95Ge	0.46	4081	2340	2920	0.379	0.667	0.478
10Li90Ge	0.54	4472	2611	3231	0.379	0.815	0.546
15Li85Ge	0.59	4779	2712	3401	0.388	0.927	0.588
20Li80Ge	0.59	4978	2846	3557	0.388	0.942	0.626
25Li75Ge	0.60	5075	2834	3581	0.393	0.939	0.638
30Li70Ge	0.66	5116	2897	3637	0.393	0.999	0.649

*Data intrapolated for all glasses from Ref.[23], except for 5Li95Ge for which the value was extrapolated from Ref.[23]

Table 3. Young's modulus (E), shear modulus (G), bulk modulus (B), Poisson's ratio (ν), Vickers Hardness (H_V), fraction of six-coordinated to total germanium (N_6), as well as fracture toughness as obtained from single-edge precracked beam measurements (K_{Ic}) and as predicted from a recent model[71] ($K_{Ic}^{Prediction}$) are presented for the probed lithium germanate glass series. Estimated average errors for E, G, B, H_V, and K_{Ic} are 0.3 GPa, 0.1 GPa, 0.2 GPa, 0.2 GPa and 0.04 MPa $m^{0.5}$, respectively. n.d. indicates that the value was not determined due to inadequate samples sizes.

Glass-ID	E (GPa)	G (GPa)	B (GPa)	ν (-)	H_V (GPa)	N_6^* (%)	K_{Ic} (MPa $m^{0.5}$)	$K_{Ic}^{Prediction}$ (MPa $m^{0.5}$)
5Li95Ge	52.7	21.0	35.9	0.26	5.4	5	0.81	0.69
10Li90Ge	67.7	27.2	43.6	0.24	6.3	11	0.85	0.78
15Li85Ge	75.5	29.9	53.0	0.26	7.4	18	0.88	0.81
20Li80Ge	83.1	33.1	57.1	0.26	7.6	20	0.84	0.78
25Li75Ge	81.9	32.1	60.2	0.27	7.1	20	0.75	0.69
30Li70Ge	82.0	32.4	57.9	0.26	6.5	20	n.d.	0.58

*Data obtained from Ref.[13]